

**Single dish performance of KVN 21-m radio telescopes :
Simultaneous observations at 22 and 43 GHz**

Sang-Sung Lee^{1,2}, Do-Young Byun^{1,2}, Chung Sik Oh^{1,2}, Seog-Tae Han^{1,2}, Do-Heung Je¹, Kee-Tae Kim^{1,2}, Seog-Oh Wi¹, Se-Hyung Cho^{1,3}, Bong Won Sohn^{1,2}, Jaeheon Kim^{1,2,4}, Jeewon Lee^{1,4}, Se-Jin Oh¹, Min-Gyu Song¹, Jiman Kang¹, Moon-Hee Chung¹, Jeong Ae Lee^{1,5}, Junghwan Oh^{1,2}, Jae-Han Bae¹, So-Young Yun¹, Jung-Won Lee¹, Bong Gyu Kim^{1,2}, Hyunsoo Chung¹, Duk-Gyoo Roh¹, Chang Hoon Lee¹, Hyun Goo Kim¹, Hyo Ryoung Kim¹, Jae-Hwan Yeom¹, Tomoharu Kurayama¹, Taehyun Jung¹, Pulun Park^{1,2}, Min Joong Kim^{1,6}, Dong-Hwan Yoon¹, and Won-Ju Kim^{1,7}

ABSTRACT

We report simultaneous multi-frequency observing performance at 22 and 43 GHz of the 21-m shaped-Cassegrain radio telescopes of the Korean VLBI Network (KVN). KVN is the first millimeter-dedicated VLBI network in Korea having a maximum baseline length of 480 km. It currently operates at 22 and 43 GHz and planned to operate in four frequency bands, 22, 43, 86, and 129 GHz. The unique quasi-optics of KVN enable simultaneous multi-frequency observations based on efficient beam filtering and accurate antenna-beam alignment at 22 and 43 GHz. We found that the offset of the beams is within < 5 arcseconds over all pointing directions of antenna. The dual polarization, cooled HEMT receivers at 22 and 43 GHz result in receiver noise temperatures less than 40 K at 21.25-23.25 GHz and 80 K at 42.11-44.11 GHz. The pointing accuracies have been measured to be 3 arcseconds in azimuth and elevation for all antennas. The measured aperture efficiencies are 65%(K)/67%(Q), 62%(K)/59%(Q), and 66%(K)/60%(Q) for the three KVN antennas, KVNYS, KVNUS, and KVNTN, respectively. The main-beam efficiencies are measured to be 50%(K)/52%(Q), 48%(K)/50%(Q), and 50%(K)/47%(Q) for KVNYS, KVNUS, and KVNTN, respectively. The estimated Moon efficiencies are 77%(K)/90%(Q), 74%(K)/79%(Q), and 80%(K)/86%(Q) for KVNYS,

¹Korean VLBI Network, Korea Astronomy and Space Science Institute, P. O. Box 88, Yonsei University, Seongsan-ro 262, Seodaemun, Seoul 120-749, Republic of Korea; sslee@kasi.re.kr

²Yonsei University Observatory, Yonsei University, Seongsan-ro 262, Seodaemun, Seoul 120-749, Republic of Korea

³Department of Astronomy, Yonsei University, Seongsan-ro 262, Seodaemun, Seoul 120-749, Republic of Korea

⁴Department of Astronomy and Space Science, Kyung Hee University, Seocheon-Dong, Giheung-Gu, Yongin, Gyeonggi-Do, 446-701

⁵University of Science and Technology, 133 Gwahangno, Yuseong-gu, Daejeon, 305-333, Republic of Korea

⁶Department of Astronomy and Space Science, Sejong University, Seoul 143-747, Korea

⁷Department of Astronomy and Space Science, Chungnam National University, Daejeon 305-764, Korea

KVNUS, KVNTN, respectively. The elevation dependence of the aperture efficiencies is quite flat for elevations $> 20^\circ$.

Subject headings: Astronomical Instrumentation

1. Introduction

The Korean VLBI Network (KVN) is the first mm-dedicated Very Long Baseline Interferometry (VLBI) network in East Asia, aiming to study the formation and death of stars, the structure and dynamics of our own Galaxy, and the nature of active galactic nuclei (AGNs) (Kim et al. 2004; Wajima et al. 2005). Simultaneous multi-frequency VLBI observations using the multi-frequency band receiver systems (Han et al. 2008) will enable us to conduct observational studies with high spatial and temporal resolution based on the technique of multi-frequency phase referencing (Asaki et al. 1998; Middelberg et al. 2005; Jung et al. 2011).

The KVN project was started in 2001 by the Korea Astronomy and Space Science Institute (KASI) with the construction of three 21-m radio telescopes in Seoul, Ulsan and Jeju island, Korea; KVN Yonsei Radio Telescope (KVNYS), KVN Ulsan Radio Telescope (KVNUS), and KVN Tanma Radio Telescope (KVNTN). The telescopes are located on the campuses of Yonsei University (Seoul), Ulsan University (Ulsan), and Tamna University (Jeju island). KVN can operate simultaneously in two radio frequency bands, 22 and 43 GHz, and will be upgraded for simultaneous four-frequency observations including the higher frequencies at 86 and 129 GHz. The maximum baseline length is ~ 480 km and the maximum angular resolution at the highest operating frequency (129 GHz) is ~ 1 milliarcsecond (mas).

A single dish first light was received by the KVN Yonsei Radio Telescope on 30 August, 2008. Following the single-dish performance evaluation observations, all three radio telescopes of KVN are now operational, and actively operated for single-dish observations of H_2O , SiO , and Methanol maser sources and extragalactic compact radio sources (Kim et al. 2010). In this paper we introduce the general aspects of the radio telescopes of the new mm-VLBI network and describe the results of the performance evaluation observations. In section 2, we describe general aspects of observing systems of the Korean VLBI Network. We report the results of the performance evaluation observations for the single dish radio telescopes in Section 3. In Section 4, some astronomical results using KVN radio telescopes are described. Our results are summarized in Section 5.

2. Telescope system

The KVN project aimed to build the first millimeter-dedicated VLBI network in Korea. KVN has a unique observing system, allowing simultaneous multi-frequency single polarization observing

in up to four frequency bands: 22, 43, 86, and 129 GHz or simultaneous multi-frequency dual polarization observing in two frequency bands out of four. A new millimeter-wave receiver optics system with three frequency-selective surfaces (dichroic filters) is an essential part of the unique system (Han et al. 2008). In this section we describe the main technical features of the KVN antennas and the observing system.

2.1. Antennas

The three 21-m antennas of KVN have been constructed by KASI under a contract with an American company, Antedo, Inc., and a Korean company, HighGain from 2004 to 2008. The antennas are located at University campuses which have the well-developed infrastructures and yield the optimal VLBI baselines for the Korean VLBI Network in the Korean peninsula. The main design features of the reflectors are determined by the fact that the antennas maintain a high surface accuracy of $< 150\mu\text{m}$ RMS and a pointing accuracy of < 4 arcsecond at wind speeds $< 10\text{m/sec}$, and the aperture efficiency should be high enough (e.g., $\sim 60\%$ at 100 GHz) as a mm-dedicated VLBI network. The KVN antennas are therefore designed to be a shaped Cassegrain-type antenna with an alt-az mount (Figure 1). The telescope has a 21-m diameter main reflector with a focal length of 6.78 m. The main reflector consists of 200 aluminium panels with a manufacturing surface accuracy of $\sim 65\mu\text{m}$. The slewing speed of the main reflector is 3°sec^{-1} , which enables fast position-switching observations. The subreflector position, tilt, and tip are remotely controlled and modeled to compensate for the gravitational deformation of the main reflector and for the sagging-down of the subreflector itself. The characteristics of the antenna systems are summarized in Table 1.

2.2. Quasi optics

A millimeter-wave receiver optics system with three frequency-selective surfaces (dichroic filters) is an essential component of the unique system enabling simultaneous multi-frequency VLBI observations in four frequency bands, 22, 43, 86 and 129 GHz. The new receiver optics system has been described by Han et al. (2008), and only its salient features will be described in this section.

In order to make simultaneous observations in the four frequency bands, receiver optics system was developed to split one signal into four using three low pass filters with nominal cutoffs at 30, 70, and 108 GHz, made of multi-layer metal meshes. The beam passing through the filter must have a large size. Furthermore since each band is to provide dual polarization observation the receiver optics should generate as little cross-polarization as possible. As usual with shaped Cassegrain antenna optics, the edge illumination at subreflector by the receiver optics should be about 17dB i.e. less than 12dB in conventional Cassegrain antenna optics, which leads to 2% spillover loss, resulting in higher illumination efficiency than obtainable from conventional Cassegrain optics fed with

a scalar horn. Satisfying such requirements usually conflicts with physical space available inside an antenna cabin. The layout of the complete receiver optics is shown in Figure 2. This configuration was determined iteratively using standard quasioptical theory (Goldsmith 1998) rather than computationally intensive physical optics method. The beam from the subreflector comes downwards to the top of the 45° flat mirror. A microwave absorber may be inserted between the flat mirror and the first Low Pass Filter for system calibration based on the chopper-wheel method (Ulich & Haas 1976). The beam from the flat mirror may be reflected, pass through, or be filtered by three Mode Selectors which consist of a flat mirror, a hole (or free space), and a Low Pass Filter (LPF). LPF1 (dichroic, cutoff \sim 70 GHz) reflects the beam for the 86/129 GHz branches and lets the beam for the 22/43 GHz branches pass through. Likewise LPF2 (cutoff \sim 30 GHz) and LPF3 (cutoff \sim 108 GHz) split beams into 22/43 GHz and 86/129 GHz respectively. The 86 and 129 GHz receivers and their corresponding quasioptical systems are currently being installed at three telescopes. Corrugated horns for 86 and 129 GHz are to be located inside cryogenic dewars while horns for 22 and 43 GHz reside outside the respective dewars. The signal losses due to the dichroic filters were measured to be $< 2\%$ (LPF1), $< 4\%$ (LPF2), $< 5\%$ (LPF1+LPF2) for the 22 GHz-band and $< 2\%$ (LPF1), $< 6\%$ (LPF2), $< 7\%$ (LPF1+LPF2) for the 43 GHz-band (Table 2).

2.3. Receivers

The 22 and 43 GHz band signals separated in the quasioptical system are coupled into the corrugated feed horns and receivers which have been built at KASI. The observing frequency bands for the receivers are 21.25-23.25 GHz and 42.11-44.11 GHz, respectively. Both receivers are dual circular polarization, cooled HEMT receivers.

As shown in Figure 3, LHCP (Left Handed Circular Polarization) and RHCP (Right Handed Circular Polarization) components of the signals are separated in septum polarizers inside the dewar of each receiver. The InP HEMT amplifiers made by Caltech and NRAO are used as the first stage LNA (Low Noise Amplifier) for the 22 and 43 GHz receivers. The equivalent noise temperatures of both amplifiers are approximately 15 K over the whole observing frequency bands. The receiver noise temperatures for three 22 GHz receivers are measured to be 30-40 K. For the 43 GHz receivers, the receiver noise temperatures are 40-50 K for one receiver and 70-80 K for the other two receivers. The increase of the receiver noise temperatures is resulted from the aggregated loss by feed horn, vacuum window, thermal isolator, and polarizer. The 43 GHz receiver with lower noise temperature is thermally isolated by a thermal isolator adopted at VLA, whereas the others by photonic bandgap isolators between dewar and polarizer. The spread of the receiver noise temperatures among 43 GHz receivers may be due to the difference of the thermal isolators. The signals are first amplified in a cooled stage and then further amplified by a room-temperature amplifier. They are then down-converted to 8-10 GHz, 1st IF (Intermediate Frequency) in the mixers using PDROs (Phase-locked Dielectric Resonator Oscillator) which are locked on the 100 MHz reference signal transmitted from the H-maser. The observing frequency bandwidth is limited within 2 GHz by BPF (Band

Pass Filter) in 1st IF. Two 1st IF signals are selected using SPDT switches. The selected signals may consist of single polarization signals at dual frequency bands or dual polarization signals at single frequency band. The signal conditioning and 2nd frequency conversion are done in the base band converter by using IRM (Image Rejection Mixer) with an image rejection ratio of 18 dB, a 8.7-10.8 GHz frequency synthesizer with a step frequency of 100 Hz, and a digital step attenuator which offers an attenuation range up to 31.5 dB in steps of 0.5 dB. The final analog output signals are limited to 512-1024 MHz by an anti-aliasing filter.

2.4. Backends

The output signal from the base band converter is split into two different paths. One goes to a digital sampler and the other to a square-law detector (or TPD). The output from the detector is amplified and input into a voltage-to-frequency converter (hereafter VFC). An embedded counter of the VFC counts the output pulse rates, which are proportional to the output power of the base band converter. The counted output pulse rates are taken every 100 millisecond by a receiver-control computer in the receiver cabin. The VFC data are used not only for calibrating the receiver gain and the sky attenuation level but also for measuring the total flux of celestial objects in continuum observation mode. An observing technique, cross scan, is used for the total flux measurements of point-like objects in continuum single dish observations at KVN. Since the technique relies on scanning with the main beam over the source position in both azimuth and elevation directions, the receiver gain and atmosphere fluctuations faster than a few seconds could not be tracked and removed. The calibration against the faster fluctuations will be improved by using a noise diode with known temperature and a faster data acquisition system.

The signals digitized by the samplers in the receiver room are processed by the KVN Data Acquisition System (DAS) to get spectra for single-dish spectroscopy observations. In VLBI operation, the digitized signals processed in the DAS are recorded onto storage media such as harddisks or magnetic tapes. As shown in Figure 4, the DAS consists of four subsystems; samplers, optical transmission system (OTS), digital filter bank (DFB) and digital spectrometer (DSM), which were manufactured by a Japanese company, Elecs Industry Co. Ltd. The samplers digitize base band signals into 2-bit data streams with four quantization levels. The output data streams of the samplers are transmitted to the observing building through optical fibers by the OTS. The DAS is configurable to various modes according to the required number of streams and bandwidths. For wideband observations, the DSM uses the output streams of the OTS, while for narrow band observations it uses the output stream of the DFB. In principle, the DFB produces 16 data streams of 16 MHz bandwidth from 4 streams of 512 MHz bandwidth. Combining more than one stream, the DFB can produce streams with wider bandwidth such as 8×32 MHz, 4×64 MHz, 2×128 MHz and 1×256 MHz. The DSM is a FX-type digital correlator and we use the auto-correlation output for spectroscopy observations. Table 3 summarizes the available spectrometer outputs of the DSM. The correlation output produced by the DSM has 8192 channels but control computer can take only

half of them. So we take full bandwidth after smoothing and binning pairs of adjacent channels, or half bandwidth by selecting 4096 contiguous channels. For example in the wide mode, we can get 4×512 MHz bandwidth spectra or 4×256 MHz bandwidth spectra. Detailed information for the KVN DAS is described in Oh et al. (2011). The DSM can calculate the cross-correlation of two input data streams and thus can be used for polarimetry. The polarimetry observation mode using KVN single-dish is currently being test, and will be described in a separate paper.

2.5. Observation control software

For single-dish operation using a KVN antenna, we support various observation modes such as sky dipping (SDIP), position switching (PS), frequency switching (FS), focusing (FOCUS), five-point mapping (FIVE), grid mapping (GRID), cross scan (CS) and on-the-fly mapping (OTF). The observed data from all observing modes except for the continuum OTF mapping are stored into a Gildas CLASS file. The continuum OTF data written in ASCII format are reduced and converted into FITS format. The observation control software was written in Python programming language and runs on IPython interpreter. A sequence of observations for many sources can be easily run by writing a simple Python script. The observation software runs on a PC running Linux. At most 8 streams of data can be simultaneously processed with a data-taking cycle of 100 milliseconds. A graphical user interface (GUI) is used for configuring devices and running observations.

3. Performance tests

On 10th October, 2008, we had first light with the KVN Yonsei radio telescope simultaneously observing H_2O and SiO masers in Orion KL at 22 and 43 GHz. The resultant spectra at both frequency bands indicate that the overall receiving system of KVN Yonsei radio telescope is functioning properly. In this section, we describe the results of single dish performance tests for KVN radio telescopes.

3.1. Antenna pointing performance

3.1.1. Beam alignment

It is very important to align the beams of different bands with other as accurately as possible. Poor beam alignment will result in the large uncertainty of flux measurements for simultaneous multi-frequency observations. Therefore the beam alignment has to be measured and corrected to satisfy the requirement that two (or four) beams should be aligned within $< 10\%$ of the FWHM of the smallest beam (e.g., 7 arcseconds for 22 and 43 GHz, and 2.5 arcseconds for 22, 43, 86, and 129 GHz).

As a first step of the beam alignment measurements, we observed some bright and compact radio sources at 22 and 43 GHz including planets and SiO maser sources for measuring the beam alignment after the setup of the quasi-optics. The beam alignments were estimated by measuring the pointing offsets at each frequency with CS and FIVE observing modes. If the measured beam alignments were larger than the requirement, we have investigated the reasons for the poor alignment. For all cases, the poor beam alignments were caused by the misalignment of the quasi-optical system including feed horns, and could be corrected by changing the angle of flat mirrors and feed horns in the quasi-optical system. Table 4 shows that the results of beam alignments with respect to the beam at 43GHz for three KVN telescopes after corrections. The beams of all KVN antennas were very well aligned in azimuth and there was no need for correction. However, beam offsets in elevation were measured to be as large as 7 arcseconds. After changing the angle of flat mirrors in the quasi-optical system, we measured the beam offsets to be < 5 arcseconds. The elevation and azimuth dependence of the beam alignments also have been investigated by observing planets and SiO masers at various elevations. We found no significant elevation dependence of the beam alignments for all KVN antennas. This implies that the quasi-optical systems and the receiver plates including the sub-plate for the 22 GHz receivers are stable against gravitational deformation.

3.1.2. Pointing accuracy

Since the beams at 22 and 43 GHz are well aligned each other, it is efficient to establish the pointing model only at 43 GHz using SiO maser sources (mostly late type stars) whose positions are very well known. As long as the alignment between two antenna beams is accurate to $< 10\%$ of the FWHM at 43 GHz, the pointing model derived from SiO maser observations at 43 GHz should ensure the pointing accuracies for both frequency bands.

A pointing model had already been obtained by observing strong SiO maser sources with a 100 GHz receiving system. These observations had been done to evaluate the performance of the antenna under the contract with the antenna manufacturer (see Kim et al. 2011). On the basis of this pointing model established at 100 GHz, a sample of 9 late type stars (Table 5) have been used continuously to improve the pointing accuracy of the telescope. Table 6 describes the accuracies of pointing models established for three KVN radio telescopes during the evaluation period 2009-2011. The root mean square (rms) of the residual pointing offsets between the observations and the pointing models are listed in azimuth (σ_{Az}), elevation (σ_{El}), and total ($\sigma_{tot} = \sqrt{\sigma_{Az}^2 + \sigma_{El}^2}$), respectively, for each epoch and telescope (see Figure 5 for an example of residual pointing offsets). Before applying a cladding system (see below for detail), the residual rms errors are < 3 arcsecond in azimuth and < 6 arcsecond in elevation. The pointing accuracies have been improved to be < 3 arcsecond in both azimuth and elevation after applying the cladding system for more efficiently insulating the antenna mount structure.

Thermal deflection of the antenna mounting structures (Yoke arms) have been investigated

in order to improve the antenna pointing accuracy. When the antenna mounting structures face directly to the Sun, thermal deflection causes the antenna pointing offsets to rapidly change from a few to ~ 40 arcseconds within an hour. The large pointing offsets result in a large uncertainty of flux measurements not only for single dish observations but also for VLBI (phase referencing) observations during day time. Therefore, we decided to apply a cladding system to the antenna mounting structures (Figure 6). New cladding system provides an efficient thermal insulation by making an air gap with its thickness of 80 mm between new and old cladding systems. New cladding systems were installed on 14 October 2010, 6 November 2010, and 24 November 2010 for KVNYS, KVNUS, and KVNTN, respectively. After applying the cladding, the pointing offsets due to thermal effects have been reduced to be less than 20 arcseconds and the time scale of the thermal effects improved to be > 5 hours. As a result, the rms residuals in the pointing model have been improved by a factor of ~ 2 (Table 6). In case of observations during day time, especially at sunrise, the pointing observations must be conducted out at least every hour for maintaining the pointing accuracy to be less than 4 arcseconds.

3.2. Antenna efficiency and gain curve

3.2.1. Antenna efficiency

Surface accuracies of the main reflectors of the KVN radio telescopes had been measured by photogrammetry at an elevation of 48° , yielding alignment surface accuracies of 50, 54, and $51 \mu\text{m}$ for the KVN Yonsei, Ulsan, and Tamna telescopes, respectively (Kim et al. 2011). The expected total surface accuracy of KVN antennas is $\sim 124 \mu\text{m}$ (Table 1) which is good to enable observations at frequencies of < 150 GHz. The surface accuracies have been verified by the 100 GHz test observations yielding aperture efficiencies of 52% and main-beam efficiencies of 46% for all three telescopes (Kim et al. 2011).

Since new receivers and quasioptical systems at 22 and 43 GHz have been installed for KVN radio telescopes, the corresponding antenna efficiencies should be measured in order to evaluate the alignment of the quasioptical systems including feed horns. The antenna efficiencies can be measured by observing primary calibrators such as planets. Since a planet can be considered as disk with uniform brightness, the measured antenna temperature, T_A^* , is related to the aperture (η_A) and beam (η_B) efficiencies as (Schloerb & Snell 1980; Rho & Jung 1999; Koo et al. 2003; Kim et al. 2011):

$$\eta_A \equiv \frac{A_e}{A_p} = \frac{\lambda^2 T_A^*}{A_p T_B \Omega_s}, \quad (1)$$

$$\eta_B \equiv \frac{\Omega_M}{\Omega_A} = \frac{T_A^* \Omega_M}{T_B \Omega_s} = \frac{A_p \Omega_M}{\lambda^2} \eta_A, \quad (2)$$

$$\Omega_s = \Omega_M \left[1 - \exp\left(-\ln 2 \left(\frac{\theta_s}{\theta_M}\right)^2\right) \right], \quad (3)$$

$$\Omega_M = 1.133 \theta_M^2, \quad (4)$$

where A_e , A_p , λ , T_B , Ω_s are the effective and physical areas of main reflector, the observing wavelength, the brightness temperature, the source solid angle, and Ω_M , Ω_A , θ_s , θ_M are the main beam solid angle, the antenna solid angle, the angular size of the source, and the size of main beam (FWHM), respectively.

Table 7 lists measurements of main beam size, θ_M , aperture efficiency, η_A , and main beam efficiency, η_B at 22 and 43 GHz over the period 2009 April–2011 March. The measured aperture efficiencies are 65%(K)/67%(Q), 62%(K)/59%(Q), and 66%(K)/60%(Q) for KVNYS, KVNUS, and KVNTN, respectively. The measurement errors of the aperture efficiencies are less than 2%. Main beam sizes were estimated from the CS or OTF observations of Venus or Jupiter as well as from the FIVE observations of strong H₂O and SiO maser sources. For each measurement of the aperture efficiency, Jupiter or Venus have been observed in CS or OTF mapping mode over various elevations when the angular sizes of the planets were smaller than the main beam size at 43 GHz. Measurements at elevations of $\geq 30^\circ$ were averaged to estimate the main beam size and the aperture efficiency with their standard deviations listed in Table 7. The main beam efficiency was calculated through its relation to the aperture efficiency (Eq.[2]).

The uncertainties of the brightness temperatures of Venus (505 ± 25 K at K-band (Butler et al. 2001) and 450 ± 32 K at Q-band (Greve et al. 1994)) and Jupiter (134 ± 4 K at K-band (Page et al. 2003) and 150 ± 12 K at Q-band (Greve et al. 1994)) dominate the error of the aperture efficiency. The predicted aperture efficiencies from the original design of the antenna with a blockage efficiency of 88% are 72% at K band and 75% at Q band. The measured aperture efficiencies are lower than these by $\leq 10\%$ and $\leq 16\%$ at each band. This is, in fact, expected from the results of the 100 GHz test observations of the KVN radio telescopes (Kim et al. 2011). The 100 GHz aperture efficiencies are 52% for the three antennas, which are lower than the designed value of 60%, due to a slightly lower blockage efficiency from the additional cladding of the subreflector supports. The aperture efficiencies at 100 GHz are similar for all antennas, whereas those at K and Q bands are different from each antenna. At K band, the aperture efficiency of KVNUS is lower than those of the others, and at Q band, KVNUS and KVNTN have lower aperture efficiencies than KVNYS. This may be because of larger misalignment of quasioptical system at KVNUS and KVNTN than that at KVNYS. The aperture efficiency is degraded if the quasioptical system is not well aligned with the antenna, although the relative beam alignment between two frequency bands is good. The alignment will be improved when new receivers at 86 and 129 GHz and corresponding quasioptical systems are installed.

The measured main beam sizes are 122''(K)/64''(Q), 123''(K)/66''(Q), and 124''(K)/64''(Q) for KVNYS, KVNUS, and KVNTN, respectively over the period 2009 April–2011 March (Table 7). The main beam sizes have no dependence on elevation and a small difference of $<4\%$ between azimuth and elevation directions. These main beam sizes are smaller by $\sim 10\%$ than the diffraction limit of 135'' at 22.235 GHz and 70'' at 43.122 GHz for uniform aperture illumination. This may result from blockage effect (Heiles et al. 2001) and/or inverse-tapered illumination of the main reflector.

These effects also result in relatively higher sidelobe levels than for the conventional Cassegrain antenna. The antenna beam patterns for all KVN antennas were measured and the beam pattern for KVNTN is shown in Figure 7. The first sidelobe levels are -13.0/-13.0 dB (K/Q), -13.0/-12.7 dB (K/Q), and -13.1/-12.7 dB (K/Q) for KVNYS, KVNUS, and KVNTN, respectively. The measured sidelobe levels are significantly higher than those (-17.6 dB) for the Cassegrain antennas with uniform illumination pattern and without blockage (Rohlfs & Wilson 2000). It should be noticed that, due to the higher sidelobe level, spectral line observation data should be carefully analyzed, taking into account possible coupling to the first sidelobe.

The main-beam efficiencies are measured to be 50%(K)/52%(Q), 48%(K)/50%(Q), and 50%(K)/47%(Q) for KVNYS, KVNUS, and KVNTN, respectively. Since the main-beam efficiency was estimated according to its relation to the aperture efficiency (Eq.[2]), the statistical errors are not estimated. However the estimation of the main-beam efficiencies are also affected by the uncertainty of the brightness temperatures of Venus and Jupiter and the measurement errors of main-beam sizes. Due to the high level sidelobes, the main-beam efficiencies are lower with respect to the aperture efficiencies than in case of conventional Cassegrain telescopes.

We measured Moon efficiencies, η_{moon} , of the KVN radio telescopes by OTF-mapping the Moon at 22 and 43 GHz. The Moon efficiencies were derived based on Linsky (1973) and Mangum (1993). The estimated Moon efficiencies are 77%(K)/90%(Q), 74%(K)/79%(Q), and 80%(K)/86%(Q) for KVNYS, KVNUS, and KVNTN, respectively (Table 8). The error of the Moon efficiency is dominated by the measurement error of antenna temperature of Moon which is as large as 1-2%.

3.2.2. Gain curve

Gain curve measurements were made in September, 2009 for KVN Yonsei, in March, 2011 for KVN Ulsan, and in December, 2010 for KVN Tamna. The elevation dependence of the aperture efficiency of the KVN 21-m radio telescopes was measured by observing bright H₂O and SiO maser sources at 22 and 43 GHz in dual polarizations (LCP and RCP) using the FIVE pointing observations. Every 10 FIVE pointing observations, the atmospheric opacity was measured and the subreflector focus was adjusted based on the pre-established model for the subreflector. In order to avoid gain degradation due to the thermal deformation of antenna, the gain curve measurements were performed at night.

The pointing offsets were corrected during the data reduction based on the results of the FIVE pointing observations. Figure 8 shows the normalized spectral line intensities of H₂O and SiO maser sources in elevations of 10° – 70° for KVN Yonsei, Ulsan, and Tamna at 22 and 43 GHz. A second order polynomial was least-square-fitted to the data. The fitted function was normalized by its maximum. Normalized gain curve has the following form: $\text{Gain}_{\text{norm}} = A_0 \times El^2 + A_1 \times El + A_2$, where El is the elevation in degree. The fitted parameters are summarized in Table 9. The gain curves at 22 GHz are quite flat at the elevations of > 20°. At 43 GHz, the antenna gains at low

elevation decrease by less than 10%.

4. Some astronomical results

4.1. Maser line surveys of the Galactic star-forming regions

Extensive simultaneous $\text{H}_2\text{O } 6_{16} - 5_{23}$ (22.23508 GHz) and $\text{CH}_3\text{OH } 7_0 - 6_1 A^+$ (44.06943 GHz) maser line surveys were carried out towards Galactic young stellar objects (YSOs) using the KVN 21-m telescopes. Because of variability of the two masers, simultaneous observations are important for comparison of their properties in detail. Bae et al. (2011) report the observational results on 180 intermediate-mass YSOs, including 14 Class 0 objects, 19 Class I objects, and 147 Herbig Ae/Be stars that are widely believed to be intermediate-mass stars in the pre-main sequence phase. H_2O and CH_3OH maser emission were detected towards 16 (9%) and 10 (6%) sources, respectively. The detection rates of both masers rapidly decrease as the central (proto)stars evolve, which is consistent with the trend for H_2O masers observed in low-mass star-forming regions (Furuya et al. 2001). This indicates that the excitation of the two masers is related to the evolutionary stage of the central object. H_2O masers usually have significantly larger relative velocities with respect to the ambient molecular gas than do CH_3OH masers. The isotropic luminosities of both masers are well correlated with the bolometric luminosities of the central (proto)stars.

The same maser line surveys were performed towards more than 1000 high-mass YSOs in different evolutionary phases: infrared dark cores, high-mass protostellar candidates, and ultracompact HII regions (Kim et al. in preparation). The detection rates of both masers significantly increase as the central objects evolve. This is contrary to the trends found in low- and intermediate-mass star-forming regions, as mentioned above. Thus the excitation of the two masers appear to be closely related to the circumstellar environments as well as the evolutionary stage of the central (proto)stars.

4.2. Late-type stars

Studies of late-type stars using the KVN Yonsei radio telescope were performed toward known stellar SiO and/or H_2O maser sources (166 both SiO and H_2O maser sources, 83 SiO-only sources, and 152 H_2O -only sources) soon after finishing the performance test observations. Both SiO and H_2O masers were detected from 112 sources at one epoch giving a detection rate of 67% toward 166 both SiO and H_2O maser sources (Kim et al. 2010), detected from 14 sources (detection rate of 17%) toward 83 SiO-only sources (Cho et al. 2011 in prep.), and detected from 62 sources (detection rate of 41%) toward 152 H_2O -only sources (Kim et al. 2011 in prep.), respectively. Some spectra simultaneously obtained in the $\text{H}_2\text{O } 6_{16} - 5_{23}$ and SiO $v = 1$ and 2, $J = 1 - 0$ transitions are shown in Figure 9. Through simultaneous observations of SiO and H_2O masers, relations between

SiO and H₂O maser properties and the dynamical connection from the pulsating atmosphere to the inner circumstellar envelope were investigated toward evolved stars. The distribution of single and double peaked profiles of H₂O maser lines were also examined in the IRAS two-color diagram. These single and double peaked H₂O maser lines can be associated with an asymmetric wind and bipolar outflows which are commonly seen in proto-planetary nebulae and planetary nebulae as suggested by Engels (2002).

4.3. Intraday variable source 0716+714

Total flux monitoring of the intraday variable source 0716+714 were made simultaneously at 21.7 GHz and 42.4 GHz with KVN Yonsei 21-m radio telescope on December 11-15, 2009 and January 4-11, 2010. An absolute calibrator, 3C 286, was observed for flux calibration, and a nearby secondary calibrator, 0836+714, observed for gain calibration. All flux measurements were done with CS (Cross Scan) mode. The total bandwidth was 500 MHz at both frequency bands. Figure 10 shows the light curves and spectral indices of 0716+714 for two epochs. In these observations, intraday variability of 0716+714 is not seen, but a monotonic increase and decrease of total flux density on longer time scale were observed. More interestingly, as the source gets brighter the spectral index becomes flatter, and vice-versa.

5. Summary

Through the performance evaluation observations in 2008-2011, we found that the KVN 21-m radio telescopes are suitable for simultaneous multi-frequency single polarization observations at 22 and 43 GHz. The dual beams at two frequencies are well aligned within < 5 arcseconds. The pointing accuracies are < 3 arcseconds in azimuth and elevation. The measured aperture efficiencies are of $> 64\%$ at 22 GHz and $> 62\%$ at 43 GHz, the main-beam efficiencies are $> 49\%$ at 22 GHz and $> 50\%$ at 43 GHz, and the estimated Moon efficiencies are > 77 at 22 GHz and $> 85\%$ at 43 GHz. The elevation dependence of the aperture efficiencies is quite flat at the elevations of $> 20^\circ$. Unique receiving systems, accurate beam alignment, and high antenna efficiencies will provide us with good opportunities for scientific observations at millimeter wavelengths not only for single radio telescope but also for Very Long Baseline Interferometry.

Further instrumentaion for KVN will include 86 and 129 GHz receivers which should be ready in late 2012. Simultaneous four-frequency observations will be ready for VLBI observations.

This work was supported by Basic Research Program (2008-2011) and also partially supported by KASI-Yonsei Joint Research Program (2010-2011) for the Frontiers of Astronomy and Space Science funded by the Korea Astronomy and Space Science Institute. We are grateful to Paul Goldsmith for careful reading and kind comments to the manuscript. We would like to thank the

anonymous referee for providing prompt and thoughtful comments that helped improve the original manuscript.

REFERENCES

- Asaki, Y., Shibata, K. M., Kawabe, R., Roh, D.-G., Saito, M., Morita, K.-I., & Sasao, T. 1998, *Radio Science*, 33, 1297
- Bae, J.-H., Kim, K.-T., Youn, S.-Y., Kim, W.-J., Byun, D.-Y., Kang, H., & Oh, C. S. 2011, *ApJS*, 196, 21
- Butler, B. J., Steffes, P. G., Suleiman, S. H., Kolodner, M. A., & Jenkins, J. M. 2001, *Icarus*, 154, 226
- Chung, M.-H., Je, D.-H., Han, S.-T., & Lee, J.-W. 2009, *JASS*, 26, 345
- Engels, D. 2002, *A&A*, 388, 252
- Furuya, R. S., Kitamura, Y., Wootten, H. A., Claussen, M. J., & Kawabe, R. 2001, *ApJ*, 559, L143
- Goldsmith, P. F., *Quasioptical Systems: Gaussian Beam Quasioptical Propagation and Applications*. (IEEE Press, New York, 1998)
- Greve, A., Steppe, H., Graham, D., & Schalinski, C. J. 1994, *A&A*, 286, 654
- Han, S.-T., Lee, J.-W., Kang, J., Je, D.-H., Chung, M.-H., Wi, S.-O., Sasao, T., & Wylde, R. 2008, *Int. J. Infrared Milli. Waves*, 29, 69
- Heiles, C., Perillat, P., Nolan, M., Lorimer, D., Bhat, R., Chosh, T., Howell, E., Lewis, M., et al. 2001 *PASP*, 113, 1247
- Jung, T., Sohn, B. W., Kobayashi, H., Sasao, T., Hirota, T., Kameya, O., Choi, Y. K., & Chung, H. S. 2011, *PASJ*, 63, 375
- Kim, H.-G., Han, S.-T., Sohn, B. W., Oh, S.-J., Je, D.-H., Wi, S.-O., & Song, M.-G. 2004, *Proc. of the 7th EVN Symp.*, ed. Bachiller, R., Colomer, F., Desmurs, J.J., de Vicente, P. (eds.), 281
- Kim, J., Cho, S.-H., Oh, C. S., & Byun, D.-Y. 2010, *ApJS*, 188, 209
- Kim, K.-T., Byun, D.-Y., Je, D.-H., Wi, S.-O., Bae, J.-H., Jung, T.-H., Lee, C.-H., Han, S.-T., et al. 2011, *JKAS*, 44, 81
- Koo, B.-C., Park, Y.-S., Hong, S. S., Yun, H.-S., Lee, S.-G., Byun, D.-Y., Lee, J.-W., Choi, H.-K., et al. 2003, *JKAS*, 36, 43

- Linsky, J. L. 1973, *ApJS*, 25, 163
- Mangum, J. G. 1993, *PASP*, 105, 117
- Mangum, J. G. 2001, *ALMA Memo*, 336
- Middelberg, E., Roy, A. L., Walker, R. C., & Falcke, H. 2005, *A&A*, 433, 897
- Oh, S.-J., Roh, D.-G., Wajima, K., Kawaguchi, N., Byun, D.-Y., Yeom, J.-H., Je, D.-H., Han, S.-T. 2011, *PASJ*, in press
- Page, L., Barnes, C., Hinshaw, G., Spergel, D. N., Weiland, J. L., Wollack, E., Bennett, C. L., Halpern, M. et al. 2003, *ApJS*, 148, 39
- Roh, D.-G., & Jung, J. H. 1999, *Publication of the Korean Astronomical Society*, 14, 123
- Rohlfs, K., & Wilson, T. L. 2000, *Tools of Radio Astronomy* (New York: Springer)
- Schloerb, F. P., & Snell, R. L. 1980, *FCRAO Report No.* 150
- Shibata, K. M, Chung, H.-S., Kamenno, S., Roh, D.-G., Umemoto, T., Kim, K.-D., Asada, K., Han, S.-T., et al. 2004, *PASJ*, 56, 475
- Ulich, B. L., & Haas, R. W. 1976, *ApJS*, 30, 247
- Wajima, K., Kim, H.-G., Han, S.-T., Roh, D.-G., Je, D.-H., Oh, S.-J., Wi, S.-O, & Korean VLBI Network Group 2005, *ArXiv e-prints*

Table 1. Specification of KVN antennas

Reflector characteristics	
Main Reflector (axisymmetric paraboloid)	
diameter	D=21.03 m
focal length	f=6.78 m
focal ratio	f/D=0.32
panels manufacturing accuracy	65 μm
alignment surface accuracy	50-54 μm
Subreflector (hyperboloid)	
diameter	d=2.25 m
manufacturing surface accuracy	50 μm
Expected total surface accuracy(EL \sim 48 $^\circ$) [†]	124 μm
panel	73 μm
alignment	60 μm
subreflector	52 μm
backup structure	62 μm
Environmental constraints	
slewing speed	3 $^\circ$ sec ⁻¹
slewing acceleration	3 $^\circ$ sec ⁻²
operating range	AZ: \pm 270 $^\circ$ EL:0 $^\circ$ – 90 $^\circ$

Note. — [†]:Aggregate surface accuracy of KVN antennas obtained from RSS (Root-Sum-Square) calculation of measured and expected contributions by main reflector panels, alignment, subreflector, and antenna backup structures. Individual contribution includes measured accuracies, measurement errors, expected thermal and wind effects.

Table 2. Singal losses by dichroic filters

Center freq. (GHz)	LPF1		LPF2		LPF1+LPF2	
	LCP (%)	RCP (%)	LCP (%)	RCP (%)	LCP (%)	RCP (%)
21.50	0.70	1.16	2.48	3.11	3.15	4.20
21.75	0.84	1.03	2.89	2.84	3.69	3.82
22.00	0.80	0.80	2.53	2.57	3.30	3.32
22.25	0.77	0.70	2.52	2.39	3.25	3.06
22.50	0.58	0.65	2.52	2.43	3.07	3.05
22.75	0.77	0.39	2.05	2.64	2.78	3.01
23.00	0.47	0.46	2.63	2.57	3.07	3.01
42.36	1.08	1.08	3.02	5.38	4.03	6.35
42.61	0.75	1.47	5.30	5.59	5.97	6.91
42.86	1.06	1.00	3.99	4.26	4.97	5.17
43.11	1.29	0.88	3.01	2.90	4.23	3.74
43.36	1.34	1.21	2.30	2.35	3.57	3.50
43.61	1.30	1.07	1.67	1.90	2.93	2.93
43.86	1.48	1.15	1.82	1.82	3.24	2.93

Note. — Frequency bandwidth for each measurement is 500 MHz. The measurements were done on 17 July, 2008.

Table 3. The Available DSM Outputs

Mode		Bandwidth ^a (MHz)	No. of Streams
Wide		512	4
Narrow	1	256	1
	2	128	2
	3	64	4
	4	32	8
	5	16	8
	6	8	8
	7	64/128	2/1
	8	32/64/128	2/1/1
	9	32/128	4/1
	10	16/32/128	2/3/1

Note. — Half bandwidth can be taken with the same number of channels for all outputs.

Table 4. Measured beam alignments of KVN antennas at 22 and 43 GHz

Telescope	Epoch	Δ_{Az} ($''$)	Δ_{El} ($''$)	Source	Obs. mode
KVNYS	Sep. 2009	-2.3	+5.6	VX Sgr	FIVE
		-0.5	+4.2	Venus	CS
		-1.4	+4.6	Jupiter	CS
KVNUS	Sep. 2009	-4.2	+3.3	VX Sgr	FIVE
		-0.7	+3.3	Venus	CS
		-3.2	+2.9	Jupiter	CS
KVNTN	Dec. 2009	+1.3	-1.3	VX Sgr	FIVE
		+3.4	-4.3	Mars	CS
		+2.4	-1.8	Jupiter	CS

Note. — Offsets of the beam at 22 GHz measured with respect to the beam at 43 GHz.

Table 5. SiO maser sources used for the pointing model

Source	α_{2000} (hh mm ss)	δ_{2000} (dd mm ss)	V_{LSR} (km/s)
R Cas	23 58 24.79	+51 23 19.5	+25.0
U Her	16 25 47.48	+18 53 33.0	–15.0
R Leo	09 47 33.49	+11 25 44.0	–1.0
IK Tau	03 53 28.87	+11 24 21.7	+37.1
o Cet	02 19 20.79	–02 58 37.4	+50.2
R Aqr	23 43 49.44	–15 17 03.9	+22.0
VX Sgr	18 08 04.05	–22 13 26.6	+5.7
W Hya	13 49 02.03	–28 22 03.0	+42.0
VY CMa	07 22 58.33	–25 46 03.2	+18.0

Table 6. Pointing accuracies of KVN antennas at 43GHz

Telescope	Epoch	σ_{Az} (μ)	σ_{El} (μ)	σ_{tot} (μ)
KVNYS	6 Mar. 2009	2.2	4.0	4.6
	18 Sep. 2009	2.2	5.0	5.5
	16 Oct. 2010 [†]	1.7	2.6	3.1
KVNUS	9 Sep. 2009	2.9	4.9	5.7
	8 Oct. 2010	2.2	5.5	5.9
	8 Nov. 2010 [†]	2.8	2.3	3.6
KVNTN	7 Dec. 2009	2.4	5.3	5.8
	17 Sep. 2010	2.6	5.7	6.3
	10 Jan. 2011 [†]	2.0	2.8	3.4

Note. — †: Pointing models established after improving the pointing accuracies by applying a cladding system.

Table 7. Efficiencies of KVN antennas at 22 and 43 GHz

Telescope	Band	Epoch	θ_M (μ)	η_A (%)	η_B (%)	Target	Ang. size (μ)	Elevation ($^\circ$)
KVNYS	K	7 Apr. 2009	124.6 ± 0.6	71.9 ± 1.2	56.6	Venus	56.1	30-59
	Q	8 Apr. 2009	65.1 ± 2.4	68.4 ± 0.8	55.3	Venus	55.5	30-59
	K	10 Nov. 2010	123.4 ± 1.2	61.4 ± 0.5	47.4	Jupiter	45.8	30-49
	Q	11 Nov. 2010	66.8 ± 0.6	64.3 ± 0.4	54.8	Jupiter	45.7	30-49
	K	16 Mar. 2011	120.9 ± 1.1	66.6 ± 0.8	49.4	Venus	14.4	30-34
	Q	16 Mar. 2011	62.1 ± 0.6	67.3 ± 1.0	49.5	Venus	14.4	30-34
	K	16 Mar. 2011	120.5 ± 1.7	61.5 ± 0.8	45.3	Jupiter	33.4	30-56
	Q	16 Mar. 2011	61.5 ± 0.9	67.7 ± 1.0	48.9	Jupiter	33.4	30-56
KVNUS	K	17 Sep. 2009	124.4 ± 3.3	64.5 ± 1.9	50.6	Venus	11.8	30-59
	Q	18 Sep. 2009	65.9 ± 3.9	67.6 ± 0.7	56.0	Venus	11.7	30-59
	K	10 Nov. 2010	124.0 ± 0.3	60.2 ± 0.5	47.0	Jupiter	45.8	30-50
	Q	10 Nov. 2010	68.2 ± 0.2	56.3 ± 0.9	50.0	Jupiter	45.8	30-50
	K	16 Mar. 2011	121.5 ± 0.9	64.6 ± 0.6	48.4	Venus	14.4	30-39
	Q	16 Mar. 2011	64.3 ± 0.7	57.1 ± 0.8	45.0	Venus	14.4	30-39
	K	16 Mar. 2011	122.9 ± 1.0	60.1 ± 0.3	46.1	Jupiter	33.4	30-58
	Q	16 Mar. 2011	66.1 ± 0.6	56.9 ± 1.1	47.4	Jupiter	33.4	45-53
KVNTN	K	15 Feb. 2011	121.4 ± 0.8	69.4 ± 0.4	51.9	Venus	17.5	30-35
	Q	15 Feb. 2011	63.3 ± 0.3	60.3 ± 0.4	46.1	Venus	17.5	30-35
	K	15 Feb. 2011	122.8 ± 0.6	63.4 ± 0.4	48.5	Jupiter	34.7	30-57
	Q	15 Feb. 2011	65.3 ± 0.4	59.5 ± 1.4	48.4	Jupiter	34.7	30-57

Note. — The brightness temperatures used of Jupiter/Venus are 134 ± 4 K (Page et al. 2003)/ 505 ± 25 K (Butler et al. 2001) at K-band and 150 ± 12 K (Greve et al. 1994)/ 450 ± 32 K (Greve et al. 1994) at Q-band. The uncertainties of the main beam size and the aperture efficiency include only statistical measurement errors.

Table 8. Moon efficiencies of KVN antennas at 22 and 43 GHz

Telescope	Band	Epoch	UT (hh:mm)	phase (days)	T_a^* (K)	η_{moon} (%)
KVNYS	K	15 Mar. 2011	18:30	10.5	184.1	76.9
	Q	15 Mar. 2011	18:30	10.5	215.0	89.6
KVNUS	K	16 Mar. 2011	19:20	11.5	181.7	73.6
	Q	16 Mar. 2011	19:20	11.5	198.8	78.8
KVNTN	K	15 Feb. 2011	12:50	12.4	202.0	79.8
	Q	15 Feb. 2011	12:50	12.4	224.6	85.7

Note. — We used 239 K and 234 K at K and Q bands for the brightness temperatures of Moon based on Linsky (1973).

Table 9. Normalized gain curve parameters of KVN antennas at 22 and 43 GHz

Telescope	Band	Epoch	A0	A1	A2
KVNYS	K	Sep. 2009	-6.70130×10^{-6}	$+4.85791 \times 10^{-4}$	0.991196
	Q	Sep. 2009	-3.94673×10^{-5}	$+3.47852 \times 10^{-3}$	0.923354
KVNUS	K	Mar. 2011	-1.39267×10^{-6}	-5.56796×10^{-4}	1.005707
	Q	Mar. 2011	-1.94371×10^{-5}	$+1.41639 \times 10^{-3}$	0.974197
KVNTN	K	Dec. 2009	-1.35247×10^{-5}	$+6.81293 \times 10^{-4}$	0.991420
	Q	Dec. 2009	-1.91393×10^{-5}	$+1.23772 \times 10^{-3}$	0.979990



Fig. 1.— Photograph of the 21-m diameter KVN Tamna radio telescope.

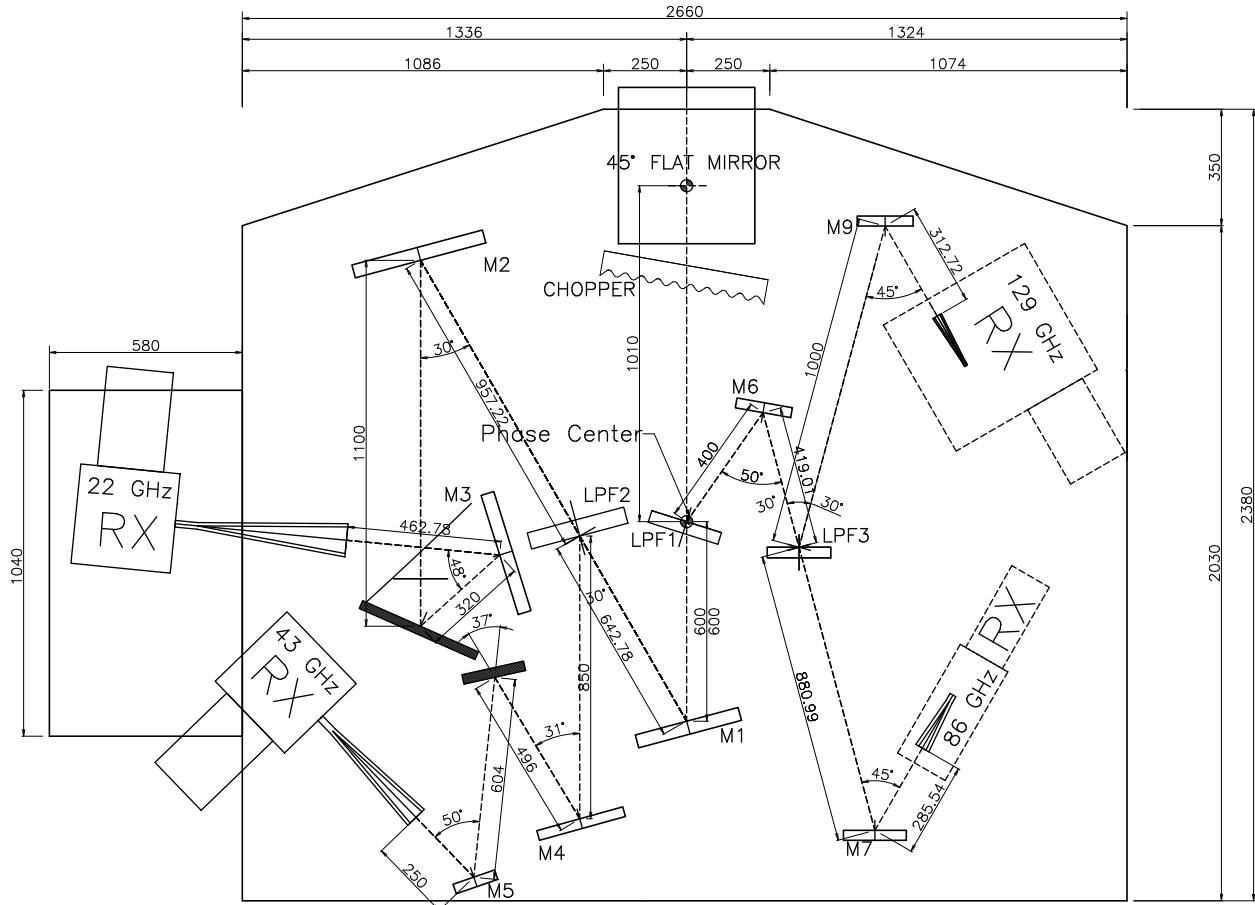


Fig. 2.— Layout of KVN receiver optics; top view, the beam from the antenna comes downwards. The 86 and 129 GHz receivers and their corresponding quasi-optical systems (M6, M7, M8, and LPF3) are currently being installed. Dimensions are given in millimeters, and angles are in degrees.

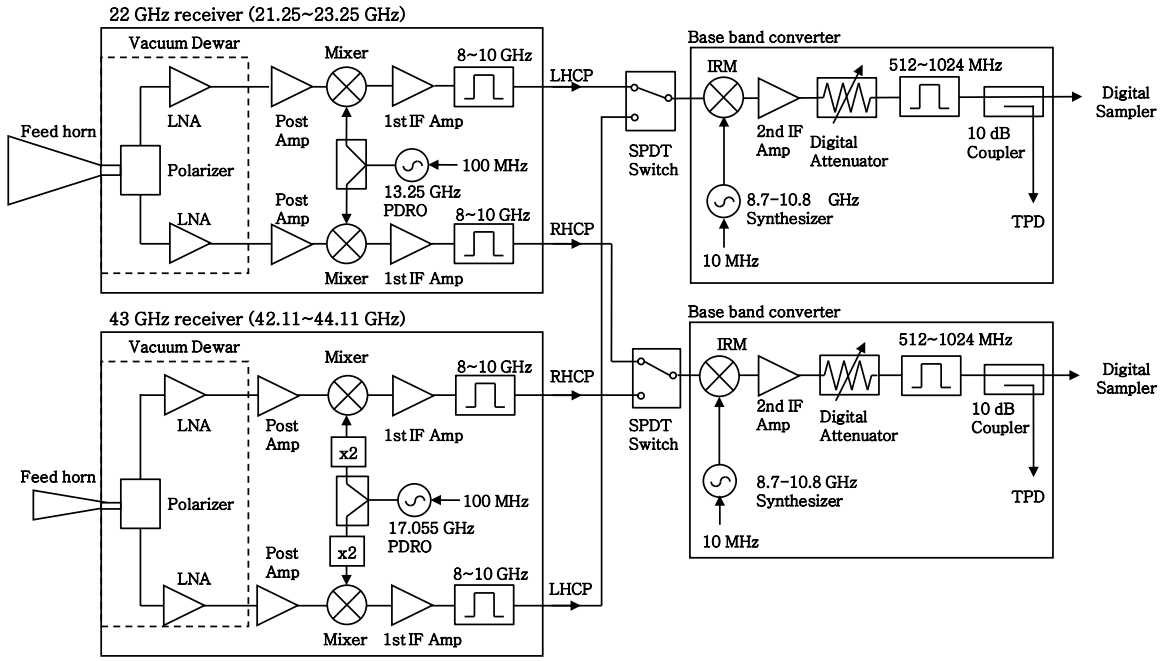


Fig. 3.— Simplified schematic diagram of 22 and 43 GHz receivers; The feed horn input signals are transmitted to the digital sampler and total power detector (TPD) through LNA (Low Noise Amplifier), following a low noise amplifier (LNA), additional amplifications, two frequency conversions, and signal leveling. Two signals are selected using two SPDT switches. PDRO: Phase-locked Dielectric Resonator Oscillator, x2: frequency doubler, LHCP: Left Handed Circular Polarization, RHCP: Right Handed Circular Polarization, SPDT: Single Pole Double Throw, IRM: Image Rejection Mixer, TPD: Total Power Detector.

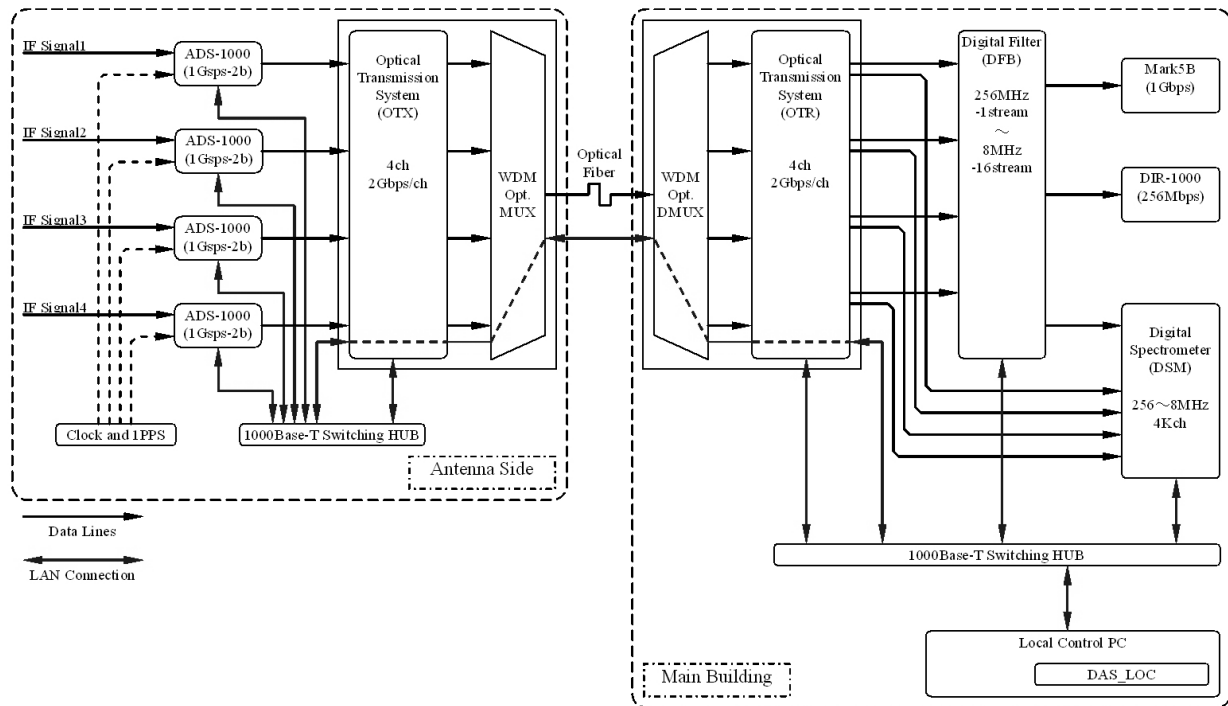


Fig. 4.— Schematic diagram of KVN Data Acquisition System. Adopted from Oh et al. (2011)

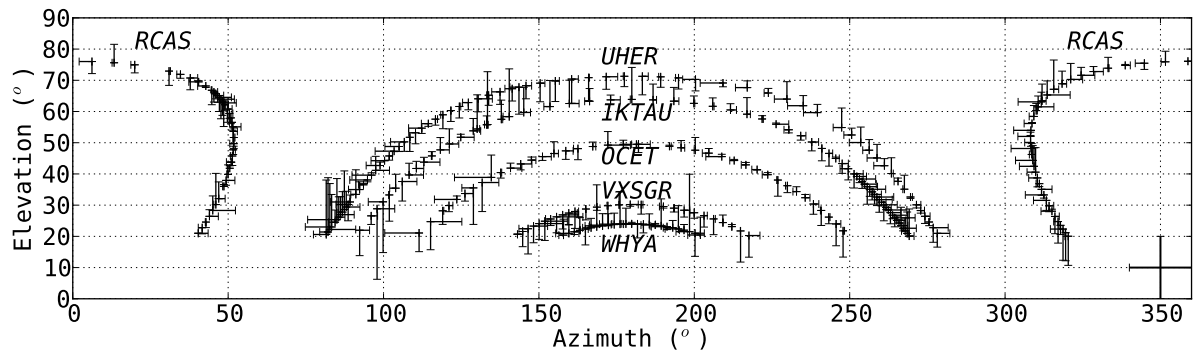


Fig. 5.— Residual pointing offsets of the pointing model for KVNYS established on 16 October, 2010 through observations of 6 SiO maser sources. Cross in the lower right corner indicates the scale of error bars at 10 arcseconds both in azimuth and elevation.

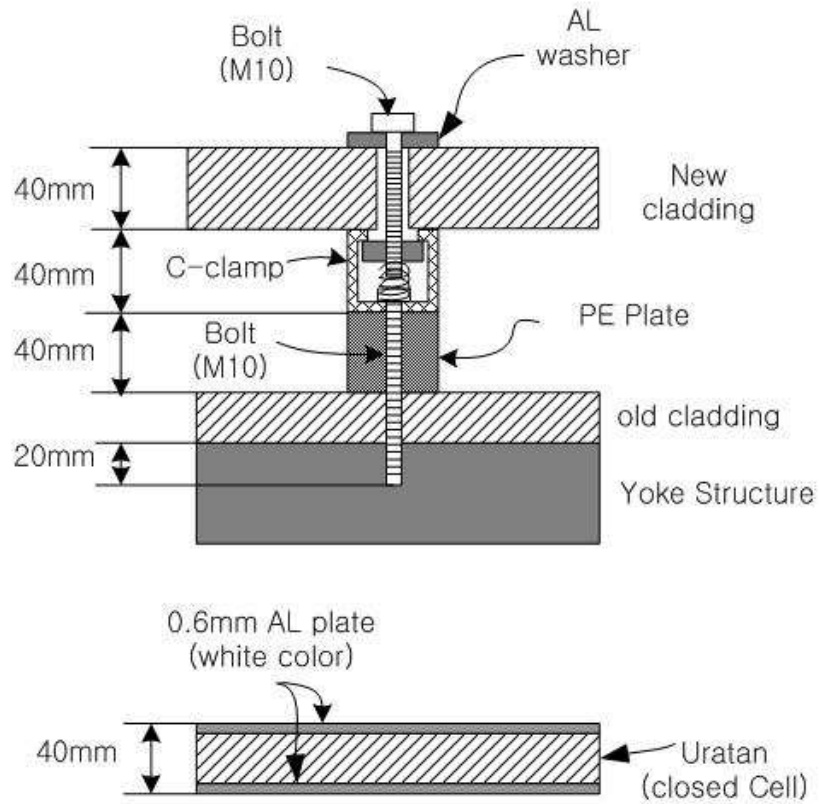


Fig. 6.— Antenna mounting structure (Yoke arms) with new cladding system (upper panel) and detailed structures of new cladding system (lower panel).

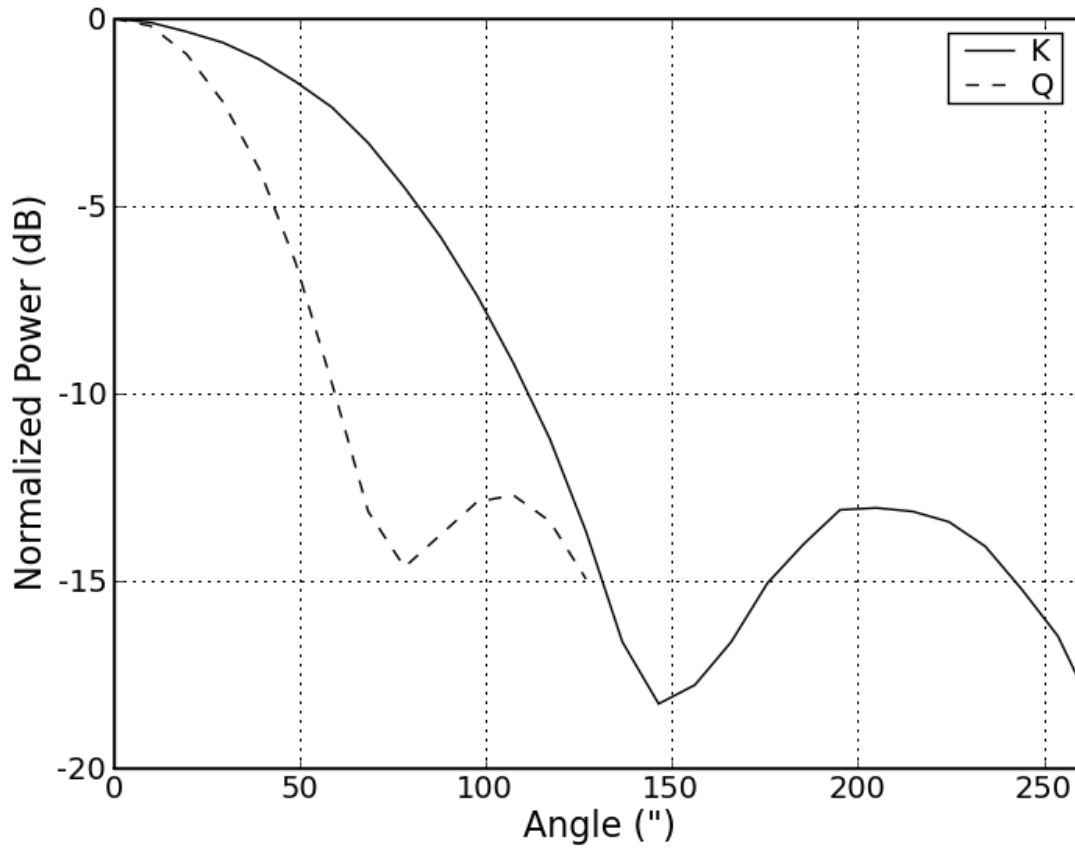


Fig. 7.— Azimuthally averaged beam patterns at K-band (solid line) and Q-band (dashed line) for KVNTN from OTF mapping observations of Jupiter.

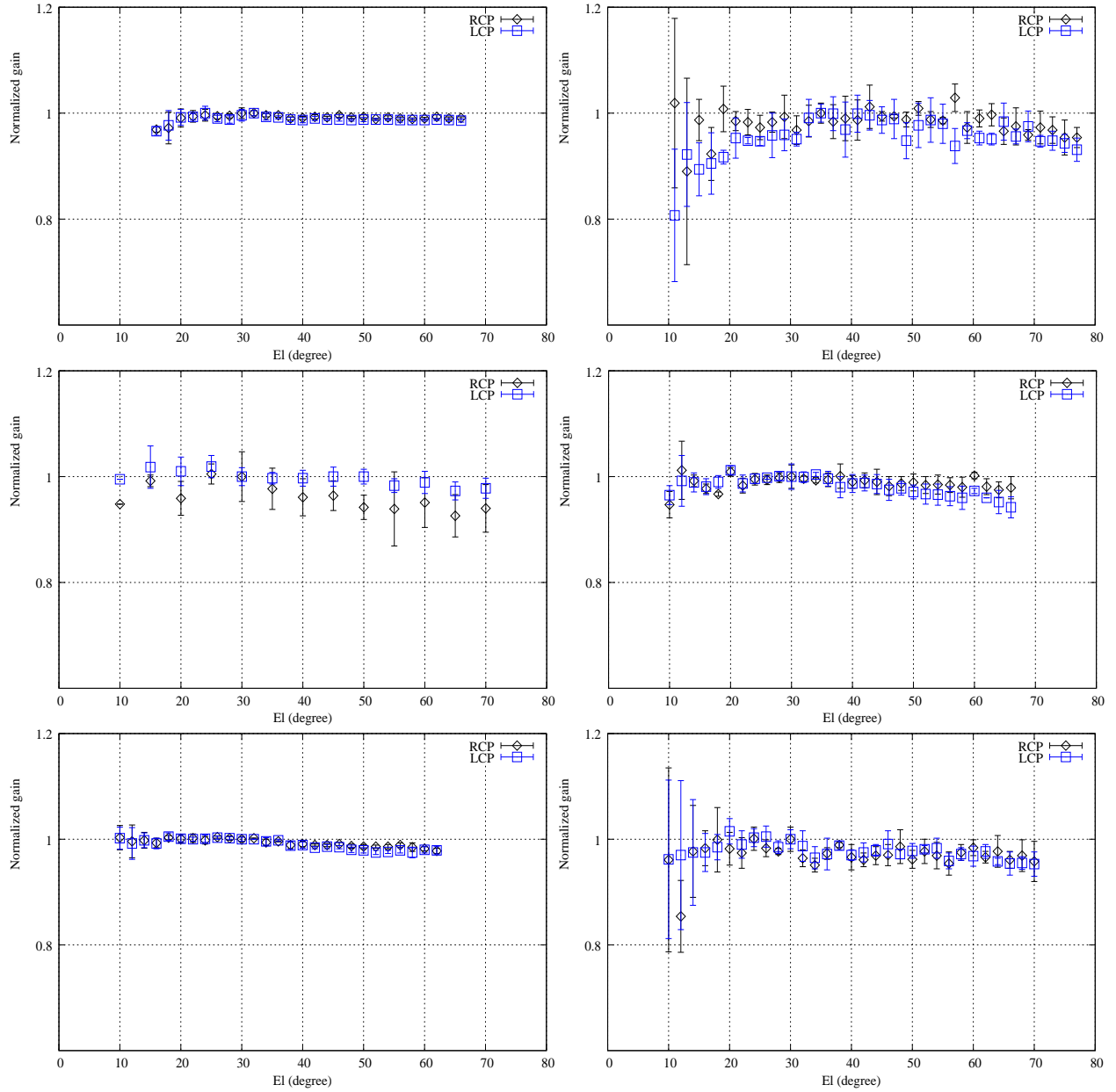


Fig. 8.— Gain curves of KVN Yonsei (upper), Ulsan (middle), Tamna (bottom) at 22 GHz (left) and 43 GHz (right).

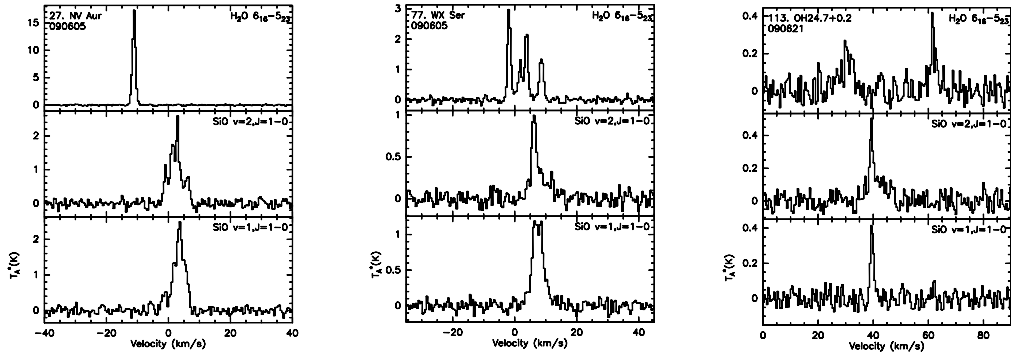


Fig. 9.— Sample spectra of three late-type stars (NV Aur, WX Ser, and OH24.7+0.2) simultaneously obtained in the H_2O $6_{16} - 5_{23}$ and SiO $v = 1$ and $2, J = 1 - 0$ transitions. Adopted from Kim et al. (2010).

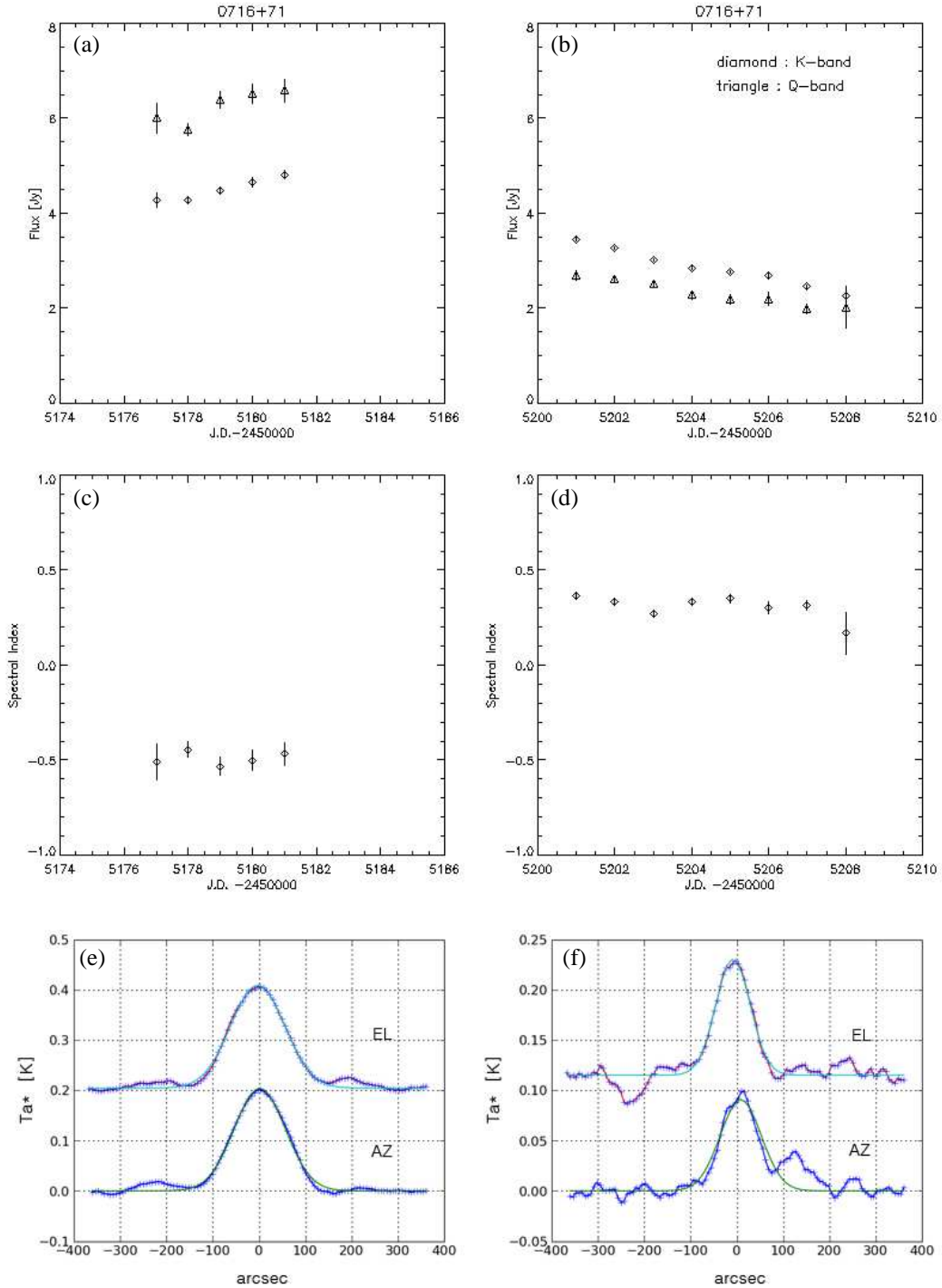


Fig. 10.— Light curves of 0716+714 in December 2009(JD 24505177-24505181) (a) and in January 2010(JD 24505201-24505208) (b), respectively, and spectral indices for the measurements in December 2009 (c) and in January 2010 (d), respectively. Examples of cross scan profiles with their gaussian fits of a flux calibrator 3C 286 taken simultaneously at 21.7 GHz (e) and 42.4 GHz (f). Error bars (one-sigma) in (a)-(d) are statistical only. Effective on-source integration times for the examples (e) and (f) are 40 and 20 seconds, respectively.